Magnomechanically controlled Goos-Hänchen shift in cavity QED

Muhammad Waseem, Muhammad Irfan,* and Shahid Qamar
Department of Physics and Applied Mathematics, PIEAS, Nilore, Islamabad 45650, Pakistan
and Center for Mathematical Sciences, PIEAS, Nilore, Islamabad 45650, Pakistan

(Received 7 November 2023; accepted 29 August 2024; published 11 September 2024)

Phenomena involving interactions among magnons, phonons, and photons in cavity magnomechanical systems have attracted considerable attention recently, owing to their potential applications in the microwave frequency range. One such important effect is the response of a probe field to such a tripartite interaction between photon-magnon-phonon. In this paper we study the Goos-Hänchen shift (GHS) of a reflected probe field in a cavity magnomechanical system. We consider a yttrium iron garnet (YIG) sphere positioned within a microwave cavity. A microwave control field directly drives the magnon mode in the YIG sphere, whereas the cavity is driven via a weak probe field. Our results show that the GHS can be coherently controlled through magnon-phonon coupling via the control field. For instance, the GHS can be tuned from positive to negative by tuning the magnon-phonon coupling. Similarly, the effective cavity detuning is another important controlling parameter for the GHS. Furthermore, we observe that the enhancement of the GHS occurs when magnon-phonon coupling is weak at resonance and when the magnon-photon coupling is approximately equal to the loss of microwave photons. Our findings may have potential significance in applications related to microwave switching and sensing.

DOI: 10.1103/PhysRevA.110.033711

I. INTRODUCTION

The cavity magnomechanical system consisting of magnons in a single-crystal yttrium iron garnet (YIG) sphere strongly coupled to the cavity mode has been theoretically proposed and experimentally demonstrated [1]. Such a system has emerged as an important frontier in the realm of cavity quantum electrodynamics (QED), drawing substantial attention in recent times [2–7]. It offers a unique platform for exploring interactions among photon, magnon, and phonon modes. Such interactions have led to some interesting outcomes such as the generation of entanglement [8,9], the preparation of squeezed states [10,11], coherent superposition, and Bell states [12].

Meanwhile, studies of the response of the microwave field to the system arising from the coupling of the magnon, phonon, and cavity microwave photon reveal magnon-induced absorption as well as magnomechanically induced transparency [13–20]. These phenomena originate from the internal constructive and destructive interference that can be interpreted by analogy with the optomechanically induced absorption and transparency, respectively, in the cavity optomechanics [21–23]. Tunable slow and fast light has also been demonstrated in cavity magnomechanics [14–17]. In this paper we focus on another crucial aspect of optical response in a cavity magnomechanical system, known as the Goos-Hänchen shift (GHS).

In classical optics, the Goos-Hänchen shift occurs when a classical electromagnetic light beam reflects from the interface of two optically different media. It is a lateral shift of the reflected light beam from the actual point of reflection at the interface and first reported in an experiment by Goos and Hänchen [24,25]. The GHS has magnificent applications in optical switching [26], optical sensors [27,28], beam splitters [26], optical temperature sensing [29], acoustics [30], seismology [31], and the theory of waveguides [32]. The GHS can be positive or negative, depending on the properties of the system under consideration. So far, various quantum systems have been investigated for the manipulation of the GHS, such as atom-cavity QED [33–35], quantum dots [36,37], cavity optomechanics [38–40], two-dimensional quantum materials [41–43], and a spin-polarized neutron reflecting from a film of magnetized material [44]. However, studies of the manipulation of the GHS in a cavity magnomechanical system, which could have possible potential applications in sensing and switching, are lacking.

In this paper we investigate the manipulation of the GHS in the reflected portion of the incident probe field in a cavity magnomechanical system using the stationary phase method. We show that the magnon-phonon coupling strength, controlled via an external microwave driving field, flexibly alters the GHS from negative to positive. The negative GHS becomes larger at weak magnon-phonon interaction strength. We also show that the GHS can be controlled by tuning the effective cavity detuning. By varying the effective detuning at zero magnon-phonon coupling strength, the GHS can be effectively tuned from positive to negative. Finally, we explore the effects in both weak- and strong-coupling limits, determined by the ratio of magnon-photon coupling to the lifetime of microwave photons. We find that the optimum value to achieve an enhanced GHS corresponds to magnon-photon

*Contact author: m.irfanphy@gmail.com

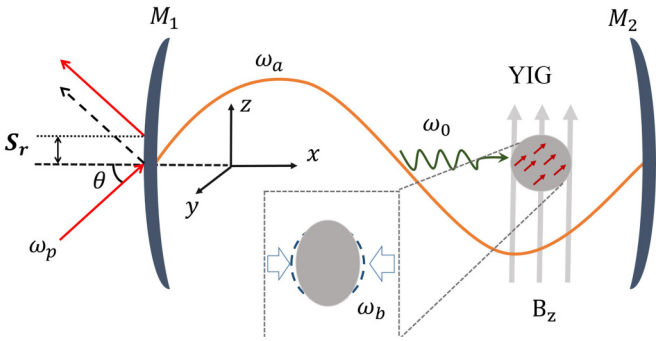

FIG. 1. Schematic diagram of the physical system. A YIG sphere is positioned inside a single-mode microwave cavity, near the maximum magnetic field of the cavity mode, and simultaneously subjected to a uniform biased magnetic field B_z. This arrangement establishes the magnon-photon coupling. A microwave field of frequency ω_0 is applied in the x direction by an external driving magnetic field B_x to enhance the magnon-phonon coupling. The magnetic fields of the cavity mode B_y, biased magnetic field B_z, and driving magnetic field B_x are mutually perpendicular at the site of the YIG sphere. The incident probe field falls in the x direction on the wall of the mirror M_1 at angle θ, which is reflected with positive or negative GHS denoted by S_r.

coupling of approximately the same strength as the cavity decay rate.

The rest of the paper is organized as follows. In Sec. II we explain the physical system. Section III presents the results and a discussion. We summarize in Sec. IV.

II. SYSTEM MODEL AND HAMILTONIAN

We consider a cavity magnomechanical system that consists of a single-mode cavity of frequency ω_a with a YIG sphere placed inside the cavity, as shown in Fig. 1. Both nonmagnetic mirrors M_1 and M_2 are kept fixed, assuming M_2 is perfectly reflecting while M_1 is partially reflecting. Both mirrors have thickness d_1 and permittivity ϵ_1. The effective cavity length is d_2 and effective cavity permittivity in the presence of a YIG sphere is ϵ_2. Therefore, our system is effectively a three-layer structure comprising two mirrors and an intracavity medium similar to atomic system [35] and cavity optomechanics [38]. In Fig. 1, a uniform bias magnetic field in the z direction is applied on the YIG sphere, which excites the magnon modes of frequency ω_m. These magnon modes are coupled with the cavity field through a magnetic dipole interaction. The excitation of the magnon modes inside the sphere varies the magnetization, resulting in the deformation of its lattice structure. This magnetostrictive force causes vibrations of the YIG sphere with phonon frequency ω_b, which establishes the magnon-phonon interaction.

Usually, the single-magnon magnomechanical coupling strength is very weak [45]. However, we consider that the magnon mode of the YIG sphere is directly driven by a strong external microwave source having frequency ω_0 and amplitude $E_d = \sqrt{5N}\gamma B_0/4$. Here γ is the gyromagnetic ratio, N is the total number of spins inside the YIG sphere, and B_0 is the magnitude of the external driving field in the x direction. This microwave driving plays the role of a control field in our model and enhances the magnomechanical (magnon-phonon) interaction of the YIG sphere. Additionally, the cavity is probed by a weak field with frequency ω_p, incident from vacuum ϵ_0 at an angle θ along the x axis. The amplitude of the probe field is $E_p = \sqrt{2P\kappa_a/\hbar\omega_p}$. Here P is the power of the probe field and κ_a is the cavity decay rate. The probe light is reflected back from the surface of the mirror M_1 with some lateral displacement along the z axis known as the GHS and denoted by S_r.

To investigate the GHS, we employ stationary phase theory, in which a well-collimated probe field with sufficiently large linewidth can be considered as a plane wave. Under the stationary phase theory, the GHS in the reflected probe laser beam is given by [46,47]

$$S_r = -\frac{\lambda_p}{2\pi}\frac{d\phi_r}{d\theta}, \tag{1}$$

where λ_p is the wavelength of the incident probe field and ϕ_r is the phase of the TE polarized reflection coefficient $R(k_z, \omega_p)$. Here $k_z = k\sin\theta$, with $k = 2\pi/\lambda_p$. Equation (1) can be expressed in a more explicit form such that [48]

$$S_r = -\frac{\lambda_p}{2\pi|R|^2}\left(\mathrm{Re}(R)\frac{d}{d\theta}\mathrm{Im}(R) + \mathrm{Im}(R)\frac{d}{d\theta}\mathrm{Re}(R)\right). \tag{2}$$

The reflection coefficient $R = R(k_z, \omega_p)$ used in Eq. (2) can be derived using standard transfer matrix theory for a three-layer structure [35] and is given by

$$R = \frac{q_0(Q_{22} - Q_{11}) - \left(q_0^2 Q_{12} - Q_{21}\right)}{q_0(Q_{22} + Q_{11}) - \left(q_0^2 Q_{12} + Q_{21}\right)}. \tag{3}$$

This transfer matrix approach is well established in the context of the GHS in atomic systems [33,35], cavity optomechanics [38,39], and quantum dots [36], among others. Here $q_0 = \sqrt{\epsilon_0 - \sin^2\theta}$ and Q_{ij} $(i, j = 1, 2)$ are the elements of the total transfer matrix

$$Q(k_z, \omega_p) = m_1(k_z, \omega_p, d_1)m_2(k_z, \omega_p, d_2)m_1(k_z, \omega_p, d_1), \tag{4}$$

where d_1 is the thickness of mirrors M_1 and M_2 and d_2 is the effective cavity length containing the YIG sphere. The element m_j relates the input and output of the electric field associated with the probe field propagating through the cavity and is given by

$$m_j(k_z, \omega_p, d_1) = \begin{bmatrix} \cos\left(k_j^x d_j\right) & i\sin\left(k_j^x d_j\right)k/k_j^x \\ i\sin\left(k_j^x d_j\right)k_j^x/k & \cos\left(k_j^x d_j\right) \end{bmatrix}, \tag{5}$$

where $k_j^x = (\omega_p/c)\sqrt{\epsilon_j - \sin^2\theta}$ is the x component of the wave number of the probe field. Here we use the definition $k = \omega_p/c$, with c the speed of light in vacuum. In addition, ϵ_j represents the susceptibility of the jth layer of the medium. The effective permittivity of the cavity is determined by the nonlinear susceptibility χ as $\epsilon_2 = 1 + \chi$. The susceptibility depends on the nonlinear interaction between the cavity field, magnon, and phonons in the presence of the microwave driving. As a result, the resonance conditions for the probe field are modified, resulting in controllable absorption and dispersion. Therefore, the reflection properties of the probe field strongly depend on the cavity magnomechanical interaction.

Next we calculate χ for the cavity magnomechanical system to study the reflection properties of the probe field. We consider the dimensions of the YIG sphere much smaller than the wavelength of the microwave so that the influence of radiation pressure in the system can be negligible. In a frame rotating with the driving frequency ω_0, the total Hamiltonian (in units of $\hbar = 1$) of the system under the rotating-wave approximation becomes

$$\begin{aligned} H &= \Delta_a a^\dagger a + \Delta_m m^\dagger m + \omega_b b^\dagger b \\ &\quad + g_{ma}(a^\dagger m + a m^\dagger) + g_{mb} m^\dagger m (b + b^\dagger) \\ &\quad + i(E_d m^\dagger + E_p e^{-i\delta t} a^\dagger - \text{H.c.}). \end{aligned} \tag{6}$$

Here a ($a^\dagger$), m ($m^\dagger$), and b ($b^\dagger$) are the annihilation (creation) operators of the cavity mode, the magnon mode, and the mechanical mode, respectively. The detunings of the cavity field, magnon mode, and probe field from the control field are $\Delta_a = \omega_a - \omega_0$, $\Delta_m = \omega_m - \omega_0$, and $\delta = \omega_p - \omega_0$, respectively. The magnomechanical coupling rate g_{mb} characterizes the interaction between the magnon and phonon modes, whereas g_{ma} determines the photon-magnon coupling strength.

To understand the dynamics of the system, we write, within the semiclassical limit, the Heisenberg-Langevin equations

$$\begin{aligned} \dot{a} &= -(i\Delta_a + \kappa_a)a - i g_{ma} m + E_p e^{-i\delta t}, \\ \dot{m} &= -(i\Delta_s + \kappa_m)m - i g_{ma} a + E_d, \\ \dot{b} &= -(i\omega_b + \gamma_b)b - i g_{mb} m^\dagger m, \end{aligned} \tag{7}$$

where

$$\Delta_s = \Delta_m + g_{mb}(b_s + b_s^*)$$

is the effective magnon-phonon detuning. In Eqs. (7) we take into account the decay of the cavity mode κ_a, the dissipation of the magnon mode κ_m, and the dissipation of the mechanical mode γ_b. Since we are interested in studying the mean response of this system to the applied probe field, we have neglected the quantum input noise and thermal noise. Using a semiclassical perturbation framework, we consider that the probe microwave field is much weaker than the control microwave field. As a result, we expand each operator as the sum of its steady-state value o_s and a small fluctuation $\delta o(t)$, where $o = (a, b, m)$. Then steady-state values of the dynamical variables become

$$\begin{aligned} a_s &= \frac{-i g_{ma} m_s}{i\Delta_a + \kappa_a}, \\ m_s &= \frac{-i g_{ma} a_s + E_d}{i\Delta_s + \kappa_m}, \\ b_s &= \frac{-i g_{mb} |m_s|^2}{i\omega_b + \gamma_b}. \end{aligned} \tag{8}$$

Considering the perturbation induced by the input probe field up to the first-order term and eliminating the steady-state values, we obtain the linearized equations of motion

$$\begin{aligned} \delta\dot{a} &= -\kappa_a \delta a - i g_{ma} \delta m + E_p e^{-ixt}, \\ \delta\dot{m} &= -\kappa_m \delta m - i g_{ma} \delta a - i g_{mb} m_s \delta b, \\ \delta\dot{b} &= -\gamma_b \delta b - i g_{mb} m_s^* \delta m, \end{aligned} \tag{9}$$

where $x = \delta - \omega_b$ is the effective detuning. For the derivation of Eqs. (9) we introduced the slowly varying operator for the linear terms of the fluctuation as $\delta a = \delta a e^{-i\Delta_a t}$, $\delta m = \delta m e^{-i\Delta_s t}$, and $\delta b = \delta b e^{-i\omega_b t}$. We also consider that the microwave field driving the magnon is at the red sideband ($\omega_b \approx \Delta_a \approx \Delta_s$) under the rotating-wave approximation, which actually leads to optimal cooling [23].

In order to solve Eqs. (9), we apply an ansatz $\delta o = o_1 e^{-ixt} + o_2 e^{ixt}$ with $o = (a, m, b)$. As a result, we obtain the amplitude a_1 of the first-order sideband of the cavity magnomechanical system for a weak probe field:[1]

$$a_1 = \frac{E_p}{(\kappa_a - ix) + \frac{g_{ma}^2(\gamma_b - ix)}{(\gamma_b - ix)(\kappa_m - ix) + G_{mb}^2}}. \tag{10}$$

Here $G_{mb} = g_{mb} m_s$ is the effective magnomechanical coupling coefficient, which can be tuned by an external magnetic field at fixed g_{mb}. Furthermore, it is not necessary to consider the expression of a_2 as it pertains to four-wave mixing with frequency $\omega_p - 2\omega_0$ for the driving field and the weak probe field. Then, using the input-output relation, we obtain $E_T = E_{in} - \kappa a_1$ [49]. The output field is related to the optical susceptibility as $\chi = E_T = \kappa_a a_1 / E_p$ [23,39,40,50,51]. Here χ is a complex expression that defines the quadrature of the field E_T containing real and imaginary parts. The quadrature is defined as $\chi = \chi_r + i\chi_i$ and can be measured by homodyne techniques. The real term displays the absorption spectrum, while the imaginary term displays the dispersion spectrum of the probe field.

III. RESULTS AND DISCUSSION

In this section we present the result of our numerical simulations. For numerical calculation, we consider the parameters from the recent experiment on a hybrid magnomechanical system [1,13]: $\omega_a = 2\pi \times 13.2$ GHz, $\omega_b = 2\pi \times 15$ MHz, $\kappa_a = 2\pi \times 2.1$ MHz, $\kappa_m = 2\pi \times 0.1$ MHz, $\gamma_b = 2\pi \times 150$ Hz, $D = 250$ μm, and the magnon-photon coupling $g_{ma} = 2\pi \times 2.0$ MHz. In order to study the GHS, we consider $\epsilon_0 = 1$, $\epsilon_1 = 2.2$, $d_1 = 4$ mm, and $d_2 = 45$ mm [1]. We consider the YIG sphere with diameter $D = 250$ μm, spin density $\rho = 4.22 \times 10^{27}$ m^{-3}, and gyromagnetic ratio $\gamma = 2\pi \times 28$ GHz/T [1,13]. For these parameters, we choose the driving magnetic field $B_0 \leqslant 0.5$ mT (which corresponds to $G_{mb}/2\pi \leqslant 1.5$ MHz) such that the system remains in the stable regime [18].

We first illustrate the output absorption spectrum as a function of effective detuning x in Fig. 2. The solid curve represents the spectrum in the absence of magnon-phonon coupling ($G_{mb} = 0$). In this condition, only the magnon mode is coupled to the cavity field mode, resulting in the splitting of the output spectrum into two Lorentzian peaks with a single dip at resonance. This spectrum is known as magnon-induced transparency. The width of this transparency window depends on magnon-photon coupling g_{ma}. Switching on the

[1]The amplitude of the output field described by Eq. (10) is equivalent to Eq. (15) in Ref. [18] under the red sideband and slowly varying approximation with phase $\phi = 0$.

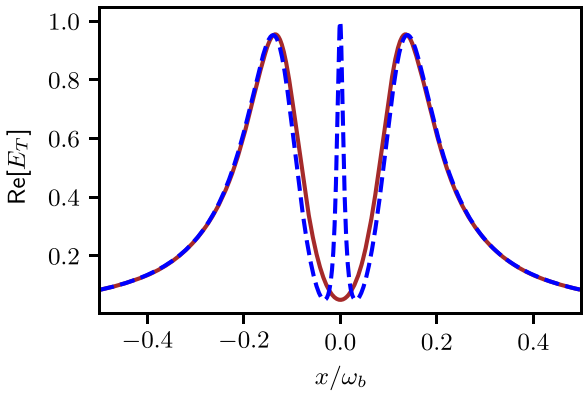

FIG. 2. Absorption spectrum of the probe field as a function of effective detuning $x = \delta - \omega_b$. Here the solid curve is at magnon-phonon coupling $G_{mb} = 0$ and the dashed curve is at $G_{mb} = 2\pi \times 0.5$ MHz. All other parameters are the same as given in the text.

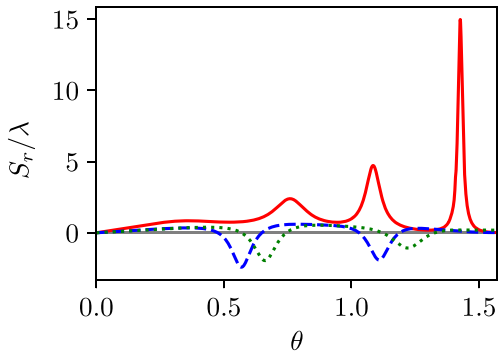

FIG. 3. Normalized GHS S_r/λ as a function of incident angle at the resonance condition $x = 0$. The solid curve shows that the GHS is always positive when $G_{mb} = 0$. The dashed and dotted curves represent the results at $G_{mb} = 2\pi \times 0.05$ and $2\pi \times 0.5$ MHz, respectively.

magnon-phonon effective coupling to $G_{mb} = 2\pi \times 0.5$ MHz by applying an external magnetic field, the single magnon-induced transparency window splits into a double window due to the nonzero magnetostrictive interaction. These results are shown by the dashed curve in Fig. 2 and are known as magnomechanically induced transparency. As the effective coupling strength G_{mb} increases from zero, the height of the central peak starts increasing, along with a slight shift to the left of the resonance point. Next we discuss the effects of control field strength, effective cavity detuning, and cavity decay rates, which are responsible for enhanced manipulation of the GHS at different incidence angles. For the sake of simplicity, we consider that the incident probe field is a plane wave.

A. Effect of the microwave driving field

The strength of the microwave driving field depends on the magnitude of an external magnetic field ($\boldsymbol{E_d} \propto \boldsymbol{B_0}$). From steady-state dynamical values [see Eq. (8)], it is evident that all excitation modes strongly depend on the strength of the microwave driving field via m_s. Similarly, the effective magnomechanical coupling coefficient G_{mb} is directly proportional to m_s at fixed g_{mb}. As a result, the output spectrum of the probe field is modified by the strength of the microwave driving field. We recall that when G_{mb} is kept zero the intracavity medium becomes transparent to the probe light beam at effective resonance $x = \delta - \omega_b = 0$. To see this effect on the GHS, we plot the GHS as a function of the probe light incident angle θ (in units of radians) in Fig. 3 at the resonance condition. It can be seen from the red curve that the GHS shift is always positive in the absence of microwave driving and exhibits three peaks. The peak of the GHS gets enhanced at a larger incident angle and is maximum at $\theta = 1.42$ rad.

When the effective magnomechanical coupling G_{mb} is turned on through an external microwave driving field, the absorption at resonance $x = 0$ starts to appear (see Fig. 2). The dashed and dotted curves in Fig. 3 show the GHS at $G_{mb} = 2\pi \times 0.05$ and $2\pi \times 0.5$ MHz, respectively. The other parameters are unchanged. We note the negative GHS in the reflected probe light beam at certain incident angles θ. Switching of the GHS from positive to negative is related to the group index of the total cavity system [33,52]. The group index is defined as the ratio of the speed of light in a vacuum to the group velocity of the reflected field and can be approximated as

$$N_g \approx \frac{1}{L}\frac{d\phi_r}{d\omega_p}, \tag{11}$$

where $L = 2d_1 + d_2$ is the total thickness of the cavity. The GHS is positive for a positive value of N_g and negative for a negative value of N_g [33]. It is already established for the case of an atomic medium that the GHS in the reflected beam is negative for the absorptive medium and positive for the transparent medium [52]. Therefore, the GHS can be coherently switched from positive to negative via an external microwave driving field. The increase of G_{mb} reduces the amplitude of the negative peaks and peaks get shifted to a higher angle as shown in Fig. 3. Therefore, in order to understand this effect more clearly, we present the contour plot of the GHS as a function of G_{mb} and angle θ in Fig. 4. The large negative GHS can be obtained at lower values of G_{mb}. The magnitude of the GHS depends on the absorption of the probe field (results shown in Fig. 2) via the reflection coefficient [Eq. (3)]. As the value of G_{mb} increases, the probe field gets more absorbed, which results in a decrease in the magnitude of the GHS.

B. Effect of detuning

Next we consider the effect of another control parameter, the effective cavity detuning on the reflected GHS. Figure 5 shows the dependence of the GHS on the effective cavity detuning and incident angles. We observe the manipulation effect on the GHS under different strengths of the microwave control field. Figure 5(a) shows the results when G_{mb} is kept zero, which means that there is no influence of the microwave driving field on the cavity. At resonance ($x = 0$), we observe a sharp transition from positive peaks to negative peaks. The magnitude of the GHS is higher at detuning relative to the resonance $x = 0$ and eventually gets smaller at larger detuning. These results provide another control mechanism of the GHS

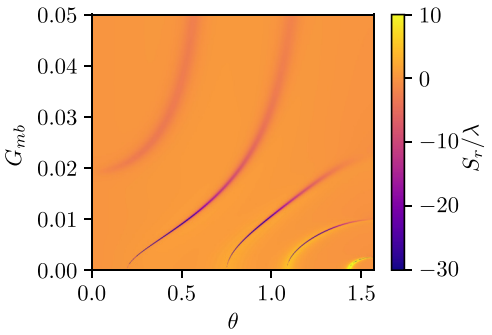

FIG. 4. Contour plot of the GHS as a function of incident angle and effective magnomechanical coupling G_{mb} (in units of $2\pi \times$ 1 MHz) at the resonance condition $x = 0$. Clearly, lower values of magnon-phonon coupling induce a larger negative GHS[2].

from positive to negative by changing the effective detuning in the absence of a microwave driving field. At a large incident angle $\theta = 1.42$ a positive shift appears in a narrow interval of detuning. In Fig. 5(b) we plot the dependence of the GHS on effective cavity detuning and incident angles of the probe light beam in the presence of the microwave control field. We note that the transition point from the negative to the positive GHS peak moves from resonance to negative effective detuning. As a result, we have a negative GHS for a relatively larger range of detuning. Away from the transition point, towards positive detuning, the amplitude of the peaks decreases and the peaks get broader.

C. Effects of weak and strong coupling

Indeed, our cavity magnomechanical system is a lossy one because the cavity photons have a limited lifetime after which they decay (lose energy) at the cavity decay rate κ_a. The cavity decay rate may be different for different microwave cavities depending on its quality factor Q. Therefore, it may also affect the reflection coefficient as well as the GHS of the reflected probe light beam. Figure 6 shows the behavior of the GHS against the normalized cavity decay rate in units of magnon-phonon coupling g_{ma} at resonance ($x = 0$). The value of the ratio κ_a/g_{ma} defines the coupling regime of the system. For instance, the strong-coupling regime corresponds to $\kappa_a/g_{ma} < 1$, whereas the weak-coupling regime corresponds to $\kappa_a/g_{ma} > 1$. Figures 6(a) and 6(b) show the results in the absence of microwave driving when $G_{mb} = 0$ at two different angles $\theta = 1.08$ and 1.42, respectively. These two angles correspond to the last two peaks of the GHS from Fig. 3 (red curve). We note that the GHS remains positive for the whole range of κ_a considered here. However, it peaks around $\kappa_a \approx g_{ma}$ and decreases symmetrically in the weak- and strong-coupling regimes. This symmetric decrease around $\kappa_a \approx g_{ma}$ becomes very fast, resulting in a narrow spectrum

[2]We used a very small step size (of both variables involved) to get the smooth and high-resolution plots in Figs. 4 and 5. As a result, some peaks or dips become quite sharp with large amplitudes. We therefore truncated the color bar limit to demonstrate the effect clearly.

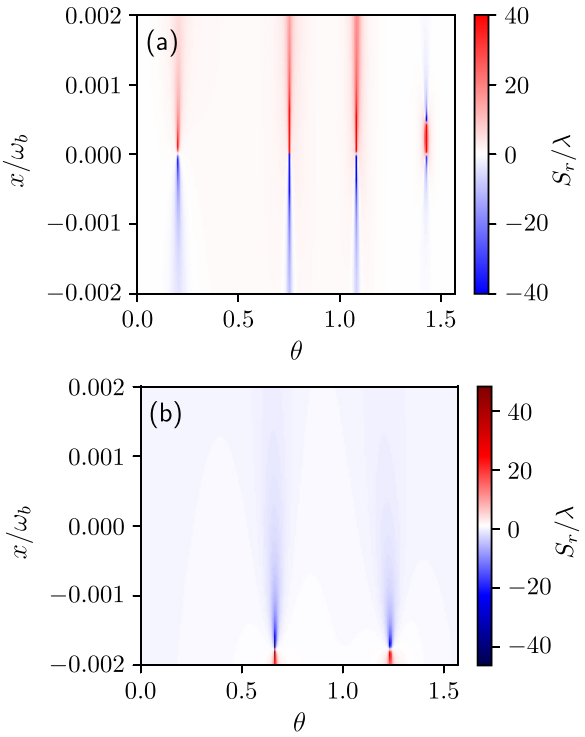

FIG. 5. Contour plot of the GHS as a function of incident angle θ and effective detuning x for (a) $G_{mb} = 0$, which indicates that the GHS can also be controlled via effective cavity detuning, and (b) $G_{mb} = 2\pi \times 1.0$ MHz, which shows that a negative GHS is larger slightly away from resonance[2].

for a larger incident angle [see Fig. 6(b)]. Figures 6(c) and 6(d) show the results in the presence of microwave driving when $G_{mb} = 2\pi \times 0.01$ and $2\pi \times 0.015$ MHz, respectively. We choose the maximum literal shift angles $\theta = 0.97$ and 0.70 from the results of Fig. 4. The GHS shift is negative and has a dip around $\kappa_a \approx g_{ma}$. Again, the width of the GHS spectrum is narrow at a larger angle. At a fixed incident angle, the peak value of the GHS depends on the reflection coefficient

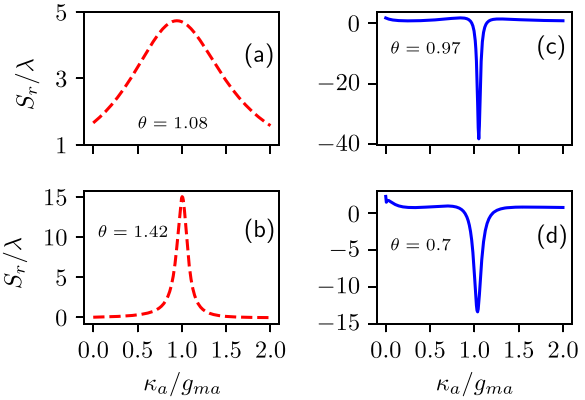

FIG. 6. Plot of the GHS as a function of cavity decay rate κ_a/g_{ma} for (a) $G_{mb} = 0$ and $\theta = 1.08$, (b) $G_{mb} = 0$ and $\theta = 1.42$, (c) $G_{mb} = 2\pi \times 0.01$ MHz and $\theta = 0.97$, and (d) $G_{mb} = 2\pi \times 0.015$ MHz and $\theta = 0.70$. For these results, we consider the resonant case $x = 0$, while the rest of the parameters are the same as given in the text.

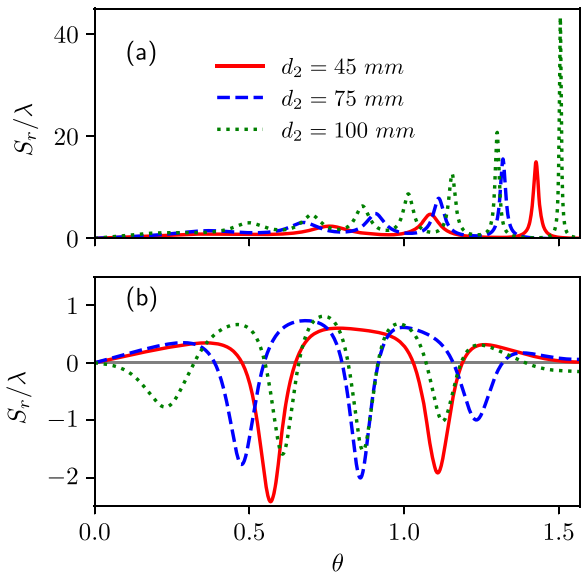

FIG. 7. Plot of the GHS as a function of incident angle for (a) $G_{mb} = 0$ and (b) $G_{mb} = 2\pi \times 0.05$ MHz at three different intracavity medium lengths. Solid, dashed, and dotted curves show the GHS at $d_2 = 45$, 70, and 100 mm, respectively. Here we consider resonance condition $x = 0$. The rest of the parameters are the same as given in the text.

R as evident from Eq. (2). At $\kappa_a \approx g_{ma}$, R approximately approaches zero, which results in the peak value of the GHS.

So far, we have discussed the effect of the driving field, which is directly related to the strength of the effective magnomechanical coupling coefficient $G_{mb} = g_{mb} m_s$ via m_s [see Eq. (8)]. Another important parameter worth studying is the cavity size. There is indeed a strong dependence of the GHS on the cavity structure, such as the total thickness of the cavity $L = 2d_1 + d_2$. Therefore, we plot the GHS as a function of incident angle θ at three different intracavity medium lengths d_2 for $G_{mb} = 0$ in Fig. 7(a) and $G_{mb} = 2\pi \times 0.05$ MHz in Fig. 7(b) at $x = 0$. Both figures show that an increase in cavity length introduces more resonance peaks and dips in the GHS as a function of the incidence angle. This dependence of the GHS on medium thickness in cavity magnomechanics is analogous to the behavior previously discussed in the GHS studies in the atomic medium [33].

IV. CONCLUSION

We have theoretically investigated the GHS in a cavity magnomechanical system where the magnon mode is excited by a coherent microwave control field. We noted the coherent manipulation of the GHS by the control microwave field. The GHS is positive at resonance in the absence of a control field. By turning on the control field, we showed that the GHS changes from positive to negative. Similarly, by modifying the effective cavity detuning in the absence of a control field, we showed the behavior of the GHS changing from positive to negative. For instance, positive detuning gives a positive GHS, while negative detuning gives a negative GHS. This symmetric behavior of the GHS around resonance, however, can be changed by turning on the control field. We also identified the optimum ratio of the microwave photon lifetime to the magnon-photon coupling to maximize the GHS. It was shown that the larger incident angles are more sensitive to this optimal ratio as compared to smaller angles.

In this work we have considered a generic cavity magnomechanical system to demonstrate the idea of the GHS. We mainly used a magnomechanically induced transparency configuration to observe the changes in the GHS of the reflected probe field. The connection between the two concepts of magnomechanically induced transparency and the magnomechanical Goos-Hänchen shift is qualitatively the same as the connection between electromagnetically induced transparency in atomic media and the corresponding Goos-Hänchen shift of the probe field due to the atomic media [33,35]. It is important to note that the idea of a tunable magnomechanically induced transparency spectrum has been demonstrated in recent experiments [1,53]. The experimental realization of the GHS in cavity magnomechanics may require design modifications in the typical experimental systems or consideration of other hybrid cavity magnomechanical systems [54–59]. We therefore believe that our analysis may be useful to investigate the GHS in cavity magnomechanical systems and may potentially lead to the development of microwave devices using the GHS. Some possible examples could be quantum switching and microwave high-precision measurement sensing.

ACKNOWLEDGMENTS

We acknowledge fruitful discussions with Dr. Muzammil Shah and Dr. Muhib Ullah.

[1] X. Zhang, C.-L. Zou, L. Jiang, and H. X. Tang, Sci. Adv. **2**, e1501286 (2016).
[2] D. Zhang, X.-M. Wang, T.-F. Li, X.-Q. Luo, W. Wu, F. Nori, and J. Q. You, npj Quantum Inf. **1**, 15014 (2015).
[3] M. Goryachev, W. G. Farr, D. L. Creedon, Y. Fan, M. Kostylev, and M. E. Tobar, Phys. Rev. Appl. **2**, 054002 (2014).
[4] Y. Li, W. Zhang, V. Tyberkevych, W.-K. Kwok, A. Hoffmann, and V. Novosad, J. Appl. Phys. **128**, 130902 (2020).
[5] O. O. Soykal and M. E. Flatté, Phys. Rev. Lett. **104**, 077202 (2010).
[6] L. Bai, M. Harder, Y. P. Chen, X. Fan, J. Q. Xiao, and C.-M. Hu, Phys. Rev. Lett. **114**, 227201 (2015).
[7] X. Zhang, C.-L. Zou, L. Jiang, and H. X. Tang, Phys. Rev. Lett. **113**, 156401 (2014).
[8] J. Li, S.-Y. Zhu, and G. S. Agarwal, Phys. Rev. Lett. **121**, 203601 (2018).
[9] B. Hussain, S. Qamar, and M. Irfan, Phys. Rev. A **105**, 063704 (2022).
[10] J. Li, S.-Y. Zhu, and G. S. Agarwal, Phys. Rev. A **99**, 021801(R) (2019).

[11] J. Li, Y.-P. Wang, J.-Q. You, and S.-Y. Zhu, Natl. Sci. Rev. **10**, nwac247 (2023).
[12] H. Y. Yuan, P. Yan, S. Zheng, Q. Y. He, K. Xia, and M.-H. Yung, Phys. Rev. Lett. **124**, 053602 (2020).
[13] X. Li, W.-X. Yang, T. Shui, L. Li, X. Wang, and Z. Wu, J. Appl. Phys. **128**, 233101 (2020).
[14] C. Kong, B. Wang, Z.-X. Liu, H. Xiong, and Y. Wu, Opt. Express **27**, 5544 (2019).
[15] B. Wang, Z.-X. Liu, C. Kong, H. Xiong, and Y. Wu, Opt. Express **26**, 20248 (2018).
[16] Z.-X. Liu, H. Xiong, and Y. Wu, IEEE Access **7**, 57047 (2019).
[17] F. Wen, B. Guo, Y. Geng, F. Yang, and B. Wu, Appl. Phys. Express **12**, 072011 (2019).
[18] T.-X. Lu, H. Zhang, Q. Zhang, and H. Jing, Phys. Rev. A **103**, 063708 (2021).
[19] A. Munir, M. Abbas, Ziauddin, W.-M. Liu, and P. Zhang, J. Opt. Soc. Am. B **40**, 1756 (2023).
[20] K. Ullah, M. T. Naseem, and O. E. Müstecaplıoğlu, Phys. Rev. A **102**, 033721 (2020).
[21] B. P. Hou, L. F. Wei, and S. J. Wang, Phys. Rev. A **92**, 033829 (2015).
[22] X. Y. Zhang, Y. Q. Guo, P. Pei, and X. X. Yi, Phys. Rev. A **95**, 063825 (2017).
[23] G. S. Agarwal and S. Huang, Phys. Rev. A **81**, 041803(R) (2010).
[24] F. Goos and H. Hänchen, Ann. Phys. (Leipzig) **436**, 333 (1947).
[25] J. Picht, Ann. Phys. (Leipzig) **395**, 433 (1929).
[26] X. Wang, C. Yin, J. Sun, H. Li, M. Sang, W. Yuan, Z. Cao, and M. Huang, Appl. Phys. Lett. **103**, 151113 (2013).
[27] C. W. Hsue and T. Tamir, J. Opt. Soc. Am. A **2**, 978 (1985).
[28] Y. Wang, Z. Cao, H. Li, J. Hao, T. Yu, and Q. Shen, Appl. Phys. Lett. **93**, 091103 (2008).
[29] C.-W. Chen, W.-C. Lin, L.-S. Liao, Z.-H. Lin, H.-P. Chiang, P.-T. Leung, E. Sijercic, and W.-S. Tse, Appl. Opt. **46**, 5347 (2007).
[30] N. F. Declercq, J. Degrieck, and O. Leroy, Appl. Phys. Lett. **85**, 4234 (2004).
[31] Z. Wang, J. Appl. Geophys. **122**, 122 (2015).
[32] I. A. White and C. Pask, Appl. Opt. **16**, 2353 (1977).
[33] Ziauddin, S. Qamar, and M. S. Zubairy, Phys. Rev. A **81**, 023821 (2010).
[34] Ziauddin and S. Qamar, Phys. Rev. A **84**, 053844 (2011).
[35] L.-G. Wang, M. Ikram, and M. S. Zubairy, Phys. Rev. A **77**, 023811 (2008).
[36] M. Idrees, M. Ullah, and L.-G. Wang, Phys. Rev. A **108**, 013701 (2023).
[37] A. Darkhosh and R. Sahandi, Laser Phys. Lett. **19**, 055207 (2022).
[38] M. Ullah, A. Abbas, J. Jing, and L.-G. Wang, Phys. Rev. A **100**, 063833 (2019).
[39] A. A. Khan, M. Abbas, Y.-L. Chaung, I. Ahmed, and Ziauddin, Phys. Rev. A **102**, 053718 (2020).
[40] Ghaisuddin, M. Abbas, A. A. Khan, H. Ali, and Ziauddin, Phys. Scr. **96**, 125104 (2021).
[41] M. Shah, Opt. Mater. Express **12**, 421 (2022).
[42] M. Shah, A. Akbar, N. A. Khan, Q. Zaman, S. Iqbal, W. Ali, M. Javed, and M. Shah, J. Opt. Soc. Am. B **39**, 1082 (2022).
[43] M. Shah, M. Sajid, and M. S. Anwar, Physica E **134**, 114819 (2021).
[44] Victor-O. de Haan, J. Plomp, T. M. Rekveldt, W. H. Kraan, A. A. van Well, R. M. Dalgliesh, and S. Langridge, Phys. Rev. Lett. **104**, 010401 (2010).
[45] Y.-P. Wang, G.-Q. Zhang, D. Zhang, T.-F. Li, C.-M. Hu, and J. Q. You, Phys. Rev. Lett. **120**, 057202 (2018).
[46] K. Artmann, Ann. Phys. (Leipzig) **437**, 87 (1948).
[47] C.-F. Li, Phys. Rev. Lett. **91**, 133903 (2003).
[48] L.-G. Wang, H. Chen, and S.-Y. Zhu, Opt. Lett. **30**, 2936 (2005).
[49] C. W. Gardiner and M. J. Collett, Phys. Rev. A **31**, 3761 (1985).
[50] F. Chen, Laser Phys. Lett. **20**, 095206 (2023).
[51] L. Li, W. Nie, and A. Chen, Sci. Rep. **6**, 35090 (2016).
[52] W. J. Wild and C. L. Giles, Phys. Rev. A **25**, 2099 (1982).
[53] J. Zhao, L. Wu, T. Li, Y.-x. Liu, F. Nori, Y. Liu, and J. Du, Phys. Rev. Appl. **15**, 024056 (2021).
[54] B. Z. Rameshti, S. V. Kusminskiy, J. A. Haigh, K. Usami, D. Lachance-Quirion, Y. Nakamura, C.-M. Hu, H. X. Tang, G. E. Bauer, and Y. M. Blanter, Phys. Rep. **979**, 1 (2022).
[55] Z.-Y. Fan, H. Qian, and J. Li, Quantum Sci. Technol. **8**, 015014 (2023).
[56] Z.-Y. Fan, H. Qian, X. Zuo, and J. Li, Phys. Rev. A **108**, 023501 (2023).
[57] D. Hatanaka, M. Asano, H. Okamoto, and H. Yamaguchi, Phys. Rev. Appl. **19**, 054071 (2023).
[58] C.-J. Yang, Q. Tong, and J.-H. An, New J. Phys. **26**, 023032 (2024).
[59] N. Zhu, X. Zhang, X. Han, C.-L. Zou, C. Zhong, C.-H. Wang, L. Jiang, and H. X. Tang, Optica **7**, 1291 (2020).